Supplementary Information

Facile Assembly of High-Solid, Responsive Liquid Photonic Crystals via RAFT-Synthesized Colloidal Nanospheres Using Rotary Evaporation

*Zhujun Wang[1, 2], Xu Zhang[1, 2], Jinping Shao[1, 2], Tianhui Zhang[1, 2], Xinyang Li[1, 2], Yi Huang[*1, 2], Jianzhong Shao[*2], San H. Thang[*3]*

1. State Key Laboratory of Bio-based Fiber Materials, Zhejiang Sci-Tech University, Hangzhou 310018, China;

2. Engineering Research Center for Eco-Dyeing and Finishing of Textiles, Ministry of Education, Zhejiang Sci-Tech University, Hangzhou, 310018, China;

3. School of Chemistry, Monash University, Clayton, Vic 3800, Australia.

* Corresponding author

E-mail address: yihuang@zstu.edu.cn; jshao@zstu.edu.cn; san.thang@monash.edu

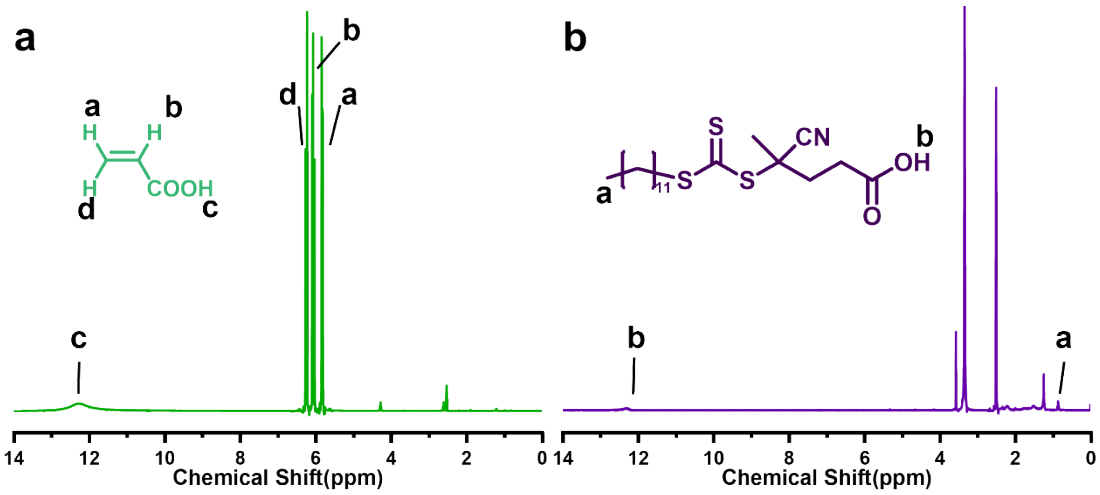

Figure S1. ^{1}H NMR of AA monomer (a) and CDPA (b).

As illustrated in Fig S1, the ^{1}H NMR spectra yield characteristic chemical shift data for acrylic acid (AA) and CDPA. Typically, the chemical shift of the proton in the carboxyl group of AA occurs around 12 ppm, while that of CDPA is observed at approximately 7 ppm. The alpha-hydrogen (α-H) proton signal of AA is noted at 6.13 ppm, and the terminal methyl group (-CH_3) of CDPA displays a peak near 0.8 ppm. These chemical shifts are crucial for assessing the conversion rates of PAA_n-CDPA and the degree of polymerization (DP).

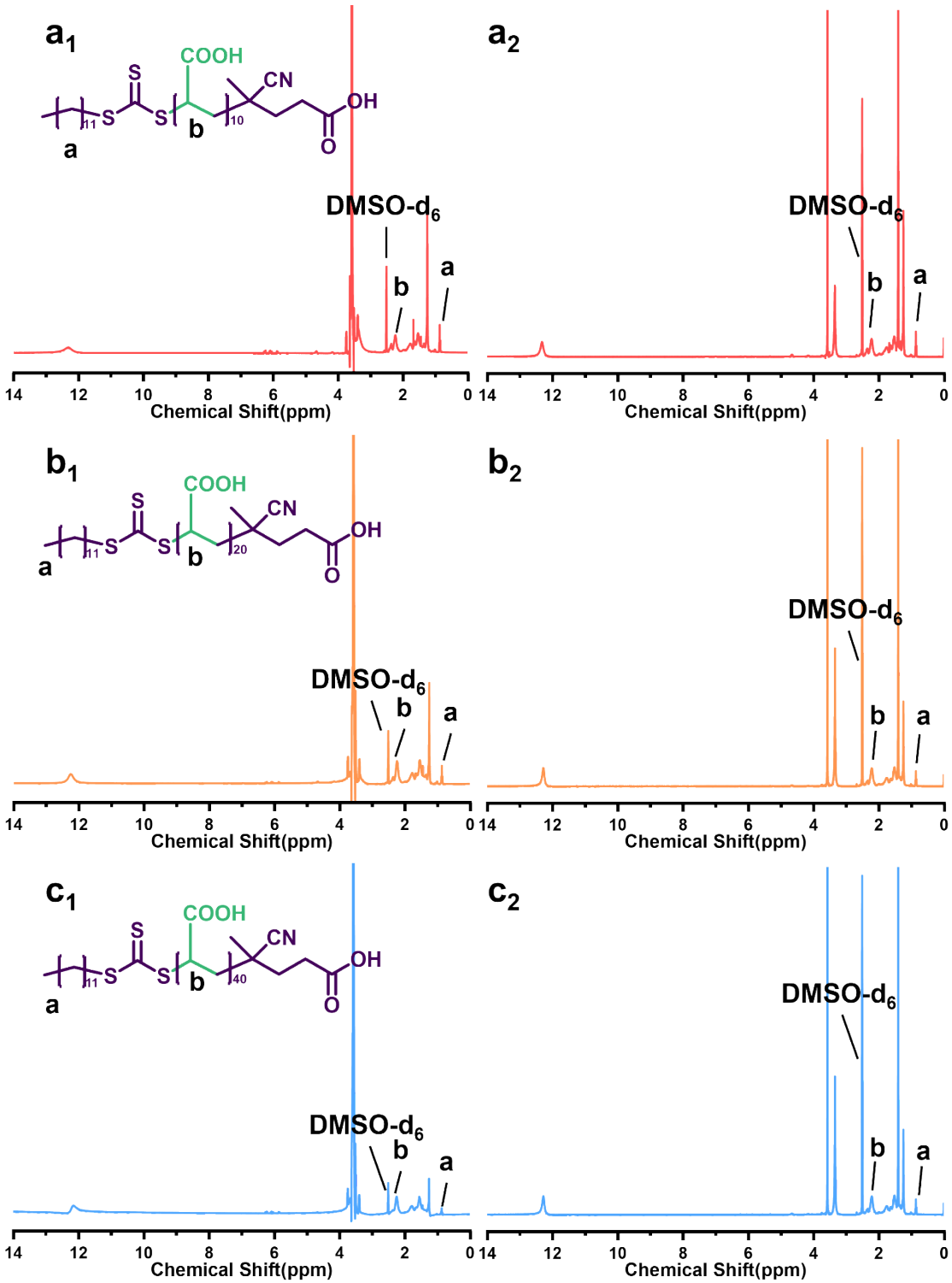

Figure S2. ^{1}H NMR of crude and purified samples of macro-CTAs PAA_{10}-CDPA (a_1 ~ a_2), PAA_{20}-CDPA (b_1 ~ b_2), and PAA_{40}-CDPA (c_1 ~ c_2).

As shown in Fig S2, the crude and purified NMR samples of PAA_{10}-CDPA, PAA_{20}-CDPA, and PAA_{40}-CDPA are presented. Using the peak area of the -CH_3 proton at position a near 0.85 ppm as the reference and setting its value to 1, it is observed that

in the crude samples, the double peaks at position b near 2.23 ~ 2.35 ppm correspond to the α-H protons of PAA, with peak areas of 9.40, 19.31, and 39.54, respectively. Additionally, impurity peaks located near 5.87 ~ 6.22 ppm are attributed to the α-H and two β-H protons of unreacted AA, showing peak areas of 0.71, 0.83, and 0.96, respectively. In the refined samples, the double peaks at position b near 2.23 ~ 2.35 ppm still correspond to the α-H protons of PAA, with peak areas of 9.01, 18.94, and 38.28, respectively. Based on these data, the DP for PAA_{10}-CDPA, PAA_{20}-CDPA, and PAA_{40}-CDPA are calculated to be 9.01, 18.94, and 38.28, respectively, with corresponding monomer conversion rates of 90.2 %, 94.3 %, and 94.7 %. These values align well with the theoretical design parameters.

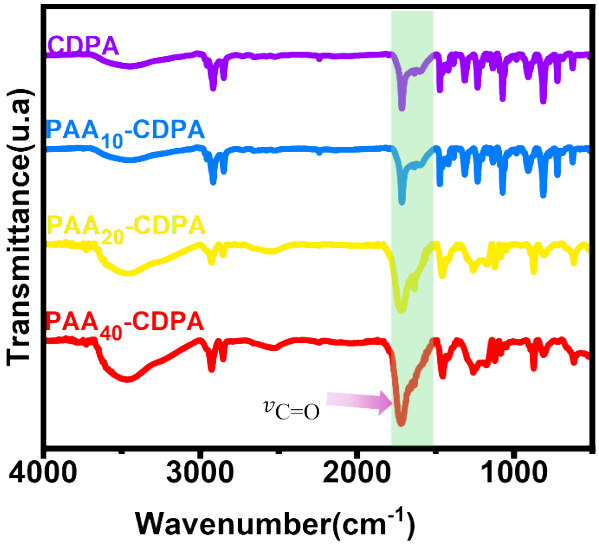

Figure S3. FTIR spectra of CDPA, PAA_{10}-CDPA, PAA_{20}-CDPA, and PAA_{40}-CDPA.

As shown in Fig S3, a comparison of the FT-IR spectra of the RAFT reagent CDPA and PAA_n-CDPA grafted with varying PAA_n block lengths demonstrates that the intensity of the C=O stretching vibration peak at 1707 cm^{-1}, attributable to carboxyl groups, exhibits a progressive increase with longer PAA_n blocks. This trend indicates that increasing amounts of AA have been successfully grafted onto CDPA, forming the corresponding PAA_n-CDPA structures.

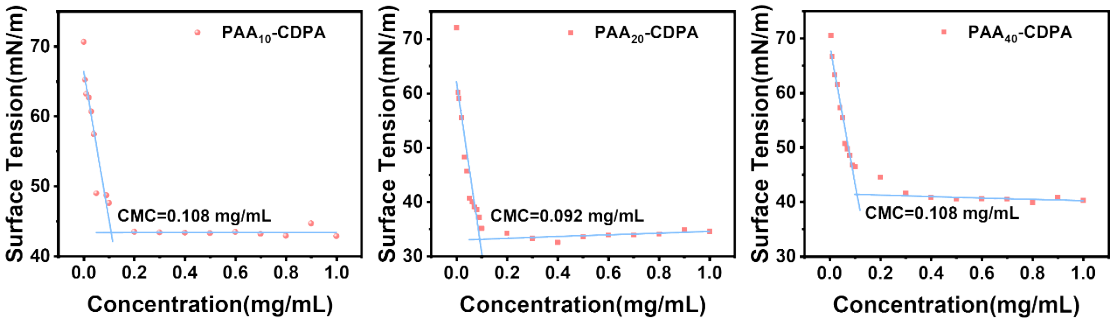

Figure S4. The surface tension of macro-CTAs PAA_n-CDPA

As shown in Figure S4, the surface activities of aqueous solutions of macro-CTAs with different DP were systematically investigated by measuring their surface tension across a concentration series. The results indicated that for all tested samples, the surface tension decreased monotonically with increasing macro-CTA concentration and eventually reached a plateau. This inflection point corresponded to the critical concentration at which micelles begin to form in large numbers. The critical micelle concentration (CMC) values for PAA_{10}-CDPA, PAA_{20}-CDPA and PAA_{40}-CDPA, determined by the plot method, are 0.108 mg/mL, 0.092 mg/mL, and 0.108 mg/mL, respectively.

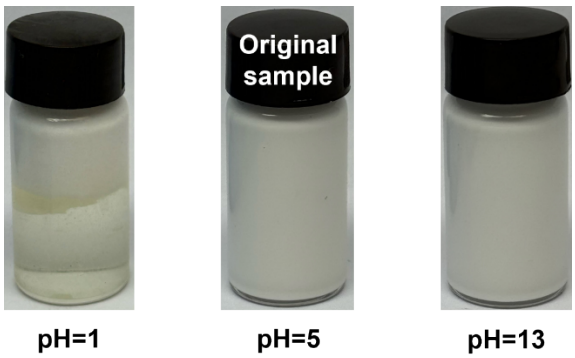

Figure S5. Dispersion stability of PAA_{20}-*b*-PS colloidal nanospheres under varying pH conditions.

As depicted in Fig S5, the synergistic effect of the continuous generation of acidic by-products from KPS decomposition and the partial ionization of carboxyl groups on the PAA_n blocks during the synthesis process resulted in a pH of approximately 5 for the newly synthesized PAA_{20}-*b*-PS colloidal nanosphere dispersion. At this pH, the -COOH groups on the surface of the colloidal nanospheres ionized to form negatively charged $-COO^-$. This ionization generated electrostatic repulsion, which kept the colloidal nanospheres uniformly dispersed, thereby preserving the stability of the

dispersion and preventing aggregation or precipitation. When the pH was decreased to 1 using a 5 mol/L HCl solution, the carboxyl groups on the colloidal nanosphere surfaces became protonated, resulting in the loss of electrostatic repulsion and leading to aggregation and precipitation of the colloidal nanospheres. After settling, the PAA_{20}-*b*-PS colloidal nanospheres, being less dense than the HCl solution, predominantly floated at the surface. When the pH was increased to 13 using a 5 mol/L NaOH solution and ultrasonic treatment was applied, the carboxyl groups on the colloidal nanosphere surfaces re-ionized, reinstating strong electrostatic repulsion and resulting in a uniformly dispersed and stable colloidal system.

Table S1. PAA_n-*b*-PS colloidal nanospheres synthesized using varying amounts of PAA_n-CDPA

CTA	PAA_n-CDPA /(wt%)	St /(wt%)	Average grain diameter/(nm)	refractive index	Average PDI
PAA_{10}-CDPA	0.614	20	180.2	1.587	0.032
	0.574	20	200.8	1.587	0.027
	0.527	20	243.9	1.587	0.058
	0.480	20	275.1	1.587	0.045
	0.402	20	310.4	1.587	0.064
PAA_{20}-CDPA	0.601	20	193.1	1.583	0.027
	0.553	20	239.0	1.583	0.040
	0.512	20	260.3	1.583	0.012
	0.457	20	292.8	1.583	0.029
	0.395	20	328.3	1.583	0.033
PAA_{40}-CDPA	0.635	20	208.5	1.575	0.053
	0.600	20	267.8	1.575	0.025
	0.558	20	283.9	1.575	0.067
	0.495	20	301.6	1.575	0.014
	0.425	20	337.4	1.575	0.052

As shown in Table S1, by controlling the amount of PAA_n-CDPA, colloidal nanosphere dispersions of PAA_n-*b*-PS with various particle sizes can be synthesized, all with polydispersity indices (PDI) below 0.08.

Table S2. The effect of rotary evaporation time on the solid content of PAA_n-*b*-PS nanospheres.

	10min	15min	20min	25min	30min	35min	40min	45min
PAA_{10}-*b*-PS	34.7%	41.3%	46.6%	50.4%	55.3%	/	/	/

PAA20-b-PS	34.3%	38.4%	42.1%	46.6%	50.2%	54.7%	/	/
PAA_{40}-*b*-PS	33.6%	36.1%	40.2%	43.8%	47.5%	51.6%	54.2%	/

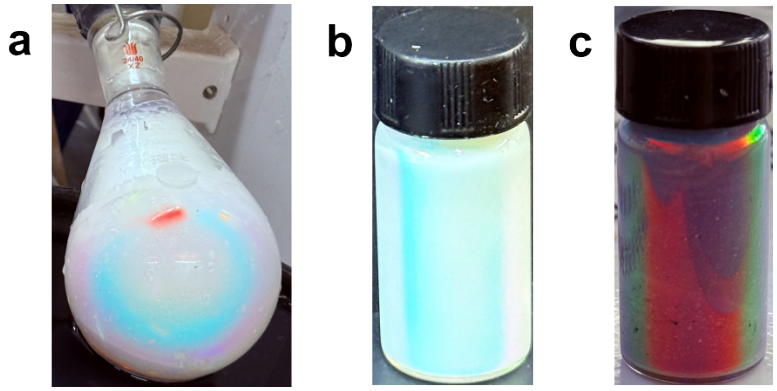

Figure S6. (a) Photograph of high-solid-content LPCs after rotary evaporation; (b), (c) Visual comparison of LPCs before and after adding CB solution, respectively.

As depicted in Table S2 and Figure S6, LPCs with different solid contents were successfully obtained by controlling the rotary evaporation time at a pH value of 8. The PAA_n-*b*-PS colloidal nanosphere dispersion was concentrated to a 55 wt% solid content through rotary evaporation, resulting in the formation of LPCs with vivid iridescence. The incorporation of CB as a broadband light absorber substantially enhanced the structural color saturation by reducing incoherent light scattering.

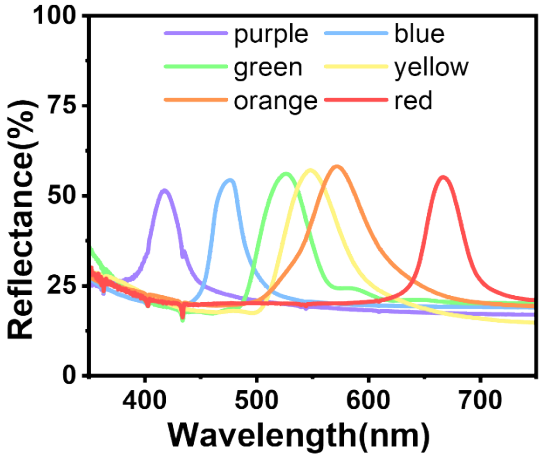

Figure S7. Reflectance spectra of LPCs exhibiting different structural color effects.

As shown in Figure S7, LPCs with a high solid content (55 wt%) can be fabricated through rotary evaporation using PAA_{20}-*b*-PS colloidal nanospheres of varying particle sizes, resulting in a spectrum of distinct hues and high color saturation.

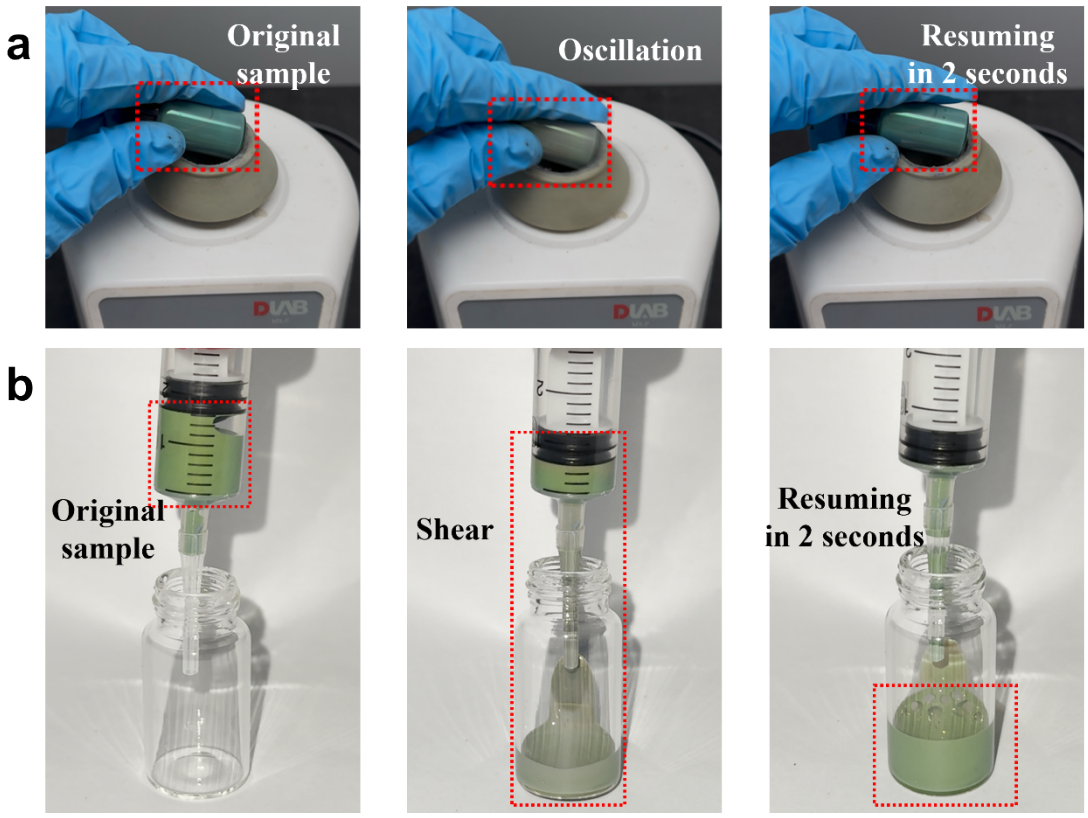

Figure S8. Dynamic recovery behavior of LPCs after shaking (a) and extrusion shearing (b).

As illustrated in Figure S8, when subjected to vigorous shaking in a vortex mixer or extrusion shearing, the PAA$_n$-*b*-PS-based LPCs experienced significant mechanical disruption. This disruption instantly demolished their pre-crystalline structure, resulting in an immediate loss of structural color. Remarkably, upon cessation of the force, the ordered domains rapidly recovered within 2 seconds through electrostatic rearrangement, effectively restoring the structural color.

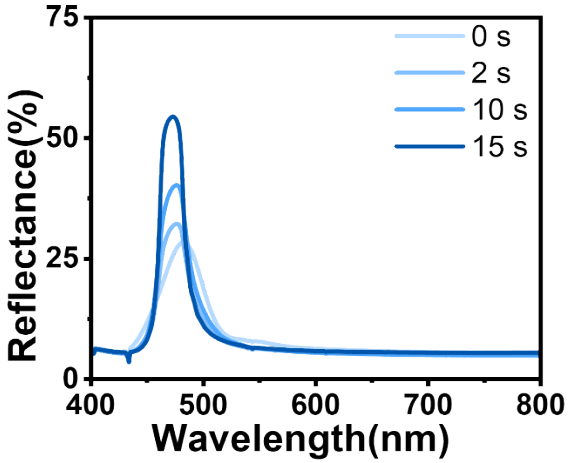

Figure S9. Reflectance spectra associated with the dynamic recovery behavior of LPCs.

As shown in Figure S9, when subjected to disturbances, the original large-scale pre-crystalline structure of the LPCs temporarily vanished; however, it rapidly reformed within 2 seconds post-disturbance, and the structural color gradually returned to normal.